Available online at www.sciencedirect.com
SCIENCE DIRECT®
Biochimica et Biophysica Acta 1655 (2004) 77–92
BIOCHIMICA ET BIOPHYSICA ACTA
BBA
www.bba-direct.com

Review

Proton-coupled electron transfer at the Q_o-site of the bc_1 complex controls the rate of ubihydroquinone oxidation

Antony R. Crofts*

Department of Biochemistry and Center for Biophysics and Computational Biology, University of Illinois at Urbana-Champaign, 419 Roger Adams Lab, 600 S. Mathews Avenue, Urbana, IL 61801, USA

Received 15 April 2003; received in revised form 29 September 2003; accepted 27 October 2003

Abstract

The rate-limiting reaction of the bc_1 complex from *Rhodobacter sphaeroides* is transfer of the first electron from ubihydroquinone (quinol, QH_2) to the [2Fe–2S] cluster of the Rieske iron–sulfur protein (ISP) at the Q_o-site. Formation of the ES-complex requires participation of two substrates (S), QH_2 and ISP_{ox}. From the variation of rate with [S], the binding constants for both substrates involved in formation of the complex can be estimated. The configuration of the ES-complex likely involves the dissociated form of the oxidized ISP (ISP_{ox}) docked at the *b*-interface on cyt *b*, in a complex in which N_ε of His-161 (bovine sequence) forms a H-bond with the quinol –OH. A coupled proton and electron transfer occurs along this H-bond. This brief review discusses the information available on the nature of this reaction from kinetic, structural and mutagenesis studies. The rate is much slower than expected from the distance involved, likely because it is controlled by the low probability of finding the proton in the configuration required for electron transfer. A simplified treatment of the activation barrier is developed in terms of a probability function determined by the Brønsted relationship, and a Marcus treatment of the electron transfer step. Incorporation of this relationship into a computer model allows exploration of the energy landscape. A set of parameters including reasonable values for activation energy, reorganization energy, distances between reactants, and driving forces, all consistent with experimental data, explains why the rate is slow, and accounts for the altered kinetics in mutant strains in which the driving force and energy profile are modified by changes in E_m and/or p*K* of ISP or heme b_L.

Keywords: Control of electron transfer; Proton transfer; bc_1 complex; Q_o-site; Marcus theory; ES-complex

1. Introduction

The X-ray crystallographic structures of the mitochondrial bc_1 complexes have provided a new perspective on functional studies [1–7]. They contain at their core the three catalytic subunits common to the bacterial enzymes. A structure at ~3.5 Å resolution of the *Rhodobacter capsulatus* complex (Berry, E. and Daldal, F., unpublished) shows that the catalytic superstructure is highly conserved, as had been expected from studies of the mechanism, which seems to be essentially the same in complexes from mitochondria and photosynthetic bacteria.

The "modified" Q-cycle of Fig. 1 accounts economically for the extensive kinetic data from studies of the turnover of the bc_1 complex measured in situ in chromatophores from photosynthetic bacteria [8–15]. The model is highly constrained by experimental data that exclude many alternative versions. Three catalytic subunits, cyt *b*, cyt c_1 and the Rieske iron–sulfur protein (ISP), house the

Abbreviations: bc_1 complex, ubiquinol:cytochrome *c* oxidoreductase (EC 1.10.2.2); b_L and b_H, low- and high-potential hemes of cytochrome *b*, respectively; cyt, cytochrome; $E_{m,\ (pH)}$, midpoint redox potential at pH indicated (pH 7 assumed if not indicated); $E_{h,\ (pH)}$, ambient redox potential at pH indicated; ESEEM, electron spin echo envelope modulation spectroscopy; HYSCORE, hyperfine sublevel correlation spectroscopy; ISP, Rieske iron–sulfur protein; ISPH, reduced ISP; ISP_{ox}, oxidized, dissociated ISP; P-phase, N-phase, aqueous phases in which the sign of the transmembrane proton gradient is positive or negative, respectively; PDB#, Protein Data Bank identifier; Q, oxidized form of quinone; QH_2, reduced form (hydroquinone, quinol) of quinone; QH·, $Q^{\cdot -}$, protonated and deprotonated forms of semiquinone; Q_i site (Q_o site), quinone reducing (quinol oxidizing) site of bc_1 complex; *Rb.*, *Rhodobacter*; RC, photosynthetic reaction center; SQ, semiquinone (with protonation state unspecified); UHDBT, 5-undecyl-6-hydroxy-4,7-dioxobenzothiazol; UHNQ, 2-undecyl-3-hydroxy-1,4-naphthoquinone

* Tel.: +1-217-333-2043; fax: +1-217-244-6615.
E-mail address: a-crofts@life.uiuc.edu (A.R. Crofts).

0005-2728/$ - see front matter © 2004 Elsevier B.V. All rights reserved.
doi:10.1016/j.bbabio.2003.10.012

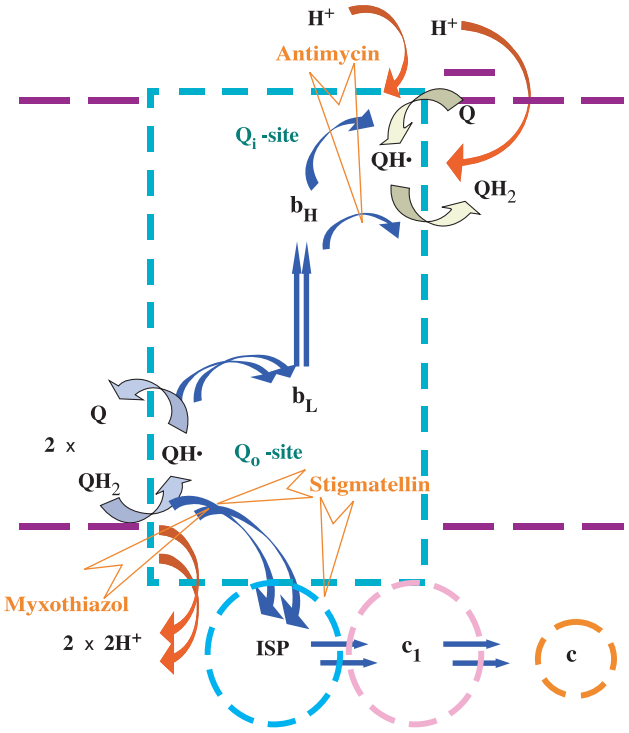

Fig. 1. The modified Q-cycle through which the bc_1 complex catalyzes the oxidation of quinol and the reduction of cytochrome (cyt) *c*. The cyt *b* subunit is represented by the dashed cyan outline, and contains the Q_o- and Q_i-sites, connected by hemes b_L and b_H. The ISP and cyt c_1 catalytic domains, and cyt *c* are represented by dashed blue, pink and orange circles. Electron transfer steps are shown by dark-blue arrows, proton release and uptake by red arrows, binding and release of quinone species by curved arrows (blue-green for Q_o-site, yellow-green for Q_i-site). Sites of inhibition are shown by open fletched arrows outlined in orange pointing from the inhibitor name to its site of action. The arrow pointing down from stigmatellin indicates that the reaction of ISPH with cyt c_1 is blocked by the interaction of ISPH with stigmatellin which binds it at the *b*-interface of the Q_o-site. See text for abbreviations.

mechanism. Two separate internal electron transfer chains connect three catalytic sites for external substrates. At one site, cyt c_1 is oxidized by cyt *c* (or c_2 in bacteria). Two catalytic sites in cyt *b* are involved in oxidation or reduction of ubiquinone. At the quinol oxidizing site (the Q_o-site), one electron from quinol is passed to the ISP, which transfers it to cyt c_1, while the semiquinone (SQ) produced is oxidized by another chain consisting of the two b-hemes of cyt *b*, in the bifurcated reaction. At the quinone-reducing site (Q_i-site), electrons from the b-heme chain are used to generate quinol. The integration of the oxidation and reduction reactions with the release or uptake of protons in the aqueous phases, allows the complex to establish a proton gradient across the membrane. Electron transfer between the two Q-sites through the b-heme chain is the main electrogenic process. The contribution of electrogenic H^+ movement is likely relatively small, because both quinone-processing sites are quite close to the aqueous phases with which they equilibrate.

The structures confirmed the main characteristics expected from previous mechanistic and structural modeling studies, but revealed several unexpected features [1–7,16–22]. The most dramatic was the evidence for a large domain movement of the ISP. On the basis of distances between donor and acceptor sites, we suggested that this movement was necessary for transfer of electrons from QH_2 to cyt c_1 [1]. Mobility of the ISP extrinsic head has been the subject of much recent work; the results have provided strong evidence that movement is required [23–31], and these aspects of structure have been extensively reviewed [22,32–34]. The movement requires specific catalysis of the separate reactions of ISP at its two reaction sites, and implies participation of five catalytic interfaces in turnover, instead of the three expected from the earlier modified Q-cycle model [18–20].

In this brief review, I will discuss the reactions at the Q_o-site, the binding of ISP with Q_o-site occupants, and the controlling role of the proton-coupled electron transfer reactions involved in ubihydroquinone (QH_2) oxidation. The question of mechanism has been highly controversial, and focused on a few key areas where none of the hypotheses proposed had appeared to be easily reconcilable with the experimental evidence. The main themes have been the nature of the enzyme–substrate complex (ES-complex) from which the electron transfer occurs, molecular details of mechanism, the site of the controlling process in determination of overall rate, and mechanism of control. The set of hypotheses presented here provides a simple explanation for many features that had appeared anomalous, and accounts economically for the experimental observations in the context of electron transfer theory and the structural information available from crystallography and spectroscopy.

1.1. Formation of the ES-complex at the Q_o-site

The overall reaction for oxidation of QH_2 at the Q_o-site of the oxidized bc_1 complex involves the [2Fe–2S] cluster of ISP_{ox} and heme b_L of cyt *b* as the immediate acceptors.

$$QH_2 + ISP_{ox} + \text{heme}b_L \leftrightarrows Q + ISPH + \text{heme}b_L^- + H^+$$

The driving force for this reaction is calculated by summing the driving forces for the two partial electron transfer reactions, $\Delta G^{o'} = -F(E_{m,\ ISP} + E_{m,\ b_L} - 2E_{m,\ Q/QH_2}) = -2.9$ kJ mol^{-1}, giving a value of $K_{eq} = 3.2$ at pH 7.0, using $E_{m,\ ISP} = 310$ mV, $E_{m,\ b_L} = -90$ mV and $E_{m,\ Q/QH_2} = 90$ mV.

A more complete description of the energy landscape requires partitioning of the driving force between a set of partial processes, including binding of substrates, activation barriers, electron and proton transfer reactions and dissociation of products.

An obvious conclusion arising from movement of the ISP is that it acts as a substrate at its two docking

$$
\begin{array}{lll}
 & Eb_L.QH_2 & \\
QH_2 \nearrow\swarrow & & \nwarrow\searrow ISP^{ox} \\
Eb_L & Eb_L.QH_2.ISP^{ox} \leftrightarrows \{ES\}^{\#} \leftrightarrows Eb_L.QH^{\bullet} + HISP^{red} & \leftrightarrows Eb_L^{-} + Q + HISP^{red} + H^{+} \\
ISP^{ox} \searrow\nwarrow & & \swarrow\nearrow QH_2 \\
 & Eb_L.ISP^{ox} &
\end{array}
$$

Scheme 1. Summary scheme to show the reactions involved in electron transfer at the Q_o-site. The formation of the ES-complex (left) occurs through two possible routes, in which one or other of the two substrates binds first, and is followed by binding of the second. After formation of the ES-complex ($Eb_L.QH_2.ISP^{ox}$), the rate-limiting first electron transfer occurs through the activated complex $\{ES\}^{\#}$, and leads to formation of an intermediate complex ($Eb_L.QH^{\cdot}$ ISPH, not shown) that breaks down by dissociation to the intermediate products, $Eb_L.QH^{\cdot}$ and $HISP^{red}$. Transfer of the second electron from $QH^{\cdot}$ to heme b_L, and dissociation to the final products (right), completes the reaction.

interfaces. It follows that two substrates contribute to formation of the ES-complex at the Q_o-site—QH_2 and ISP_{ox}, as shown in Scheme 1. The scheme summarizes our working hypothesis for the reaction sequence for QH_2 oxidation [16–20,35–39].

From the structure of the stigmatellin-containing complex, we suggested that the ES-complex was formed between QH_2 in a position at the end of the pocket distal from heme b_L, similar to that found for stigmatellin, and ISP_{ox} docked in the position seen for ISPH in the stigmatellin structure. A likely configuration involved a H-bond between the ring −OH of the quinol, and the N_ε of ISP His-161 (Fig. 2). Because of the difference in pK_a values for QH_2 (pK >11.5) and the ISP (pK ~ 7.6), the quinol-OH was suggested as the most likely H-bond donor [35,40].

This conclusion was at variance with previous speculations about the nature of the ES-complex, and the bond formed. These had been heavily influenced by early experiments of Rich and Bendall [41] in which the rate of oxidation of QH_2 by cyt c in solution was shown to be strongly accelerated by raising the pH over the range up to 11. The results were interpreted as showing that dissociation of QH_2 to the quinol anion, QH^-, was a prerequisite step before electron transfer could occur. Extrapolating this to the enzyme catalyzed reaction led to the suggestion of two alternative scenarios for formation of the ES-complex:

$$QH_2 \leftrightarrows QH^- + H^+ \leftrightarrows E\ QH^- \rightarrow E + P$$

$$QH_2 + E \leftrightarrows E\ QH_2 \leftrightarrows E\ QH^- + H^+ \rightarrow E + P$$

The first of these was incorporated into the "proton-gated affinity change" mechanism of Link [42], in which an explicit role of His-161 in its protonated form was postulated as providing a base to favor the binding of the quinol anion. The second reaction sequence was incorporated into the "proton-gated charge transfer" model of Brandt [43,44]. In both mechanisms, electron transfer proceeded only after deprotonation of QH_2, and release of the proton occurred to the aqueous phase. However, the experimental justification for this was ambiguous. The enzyme-catalyzed reaction showed a stimulation over the pH range 5.0–8.0, as expected, but in contrast to the reaction in solution, there was a strong *decrease* in rate over the pH range above 8.0 [44,45].

With our suggestion that formation of the ES-complex involved the dissociated form of the ISP_{ox}, bound to the neutral quinol, the strong dependence on pH of the rate of

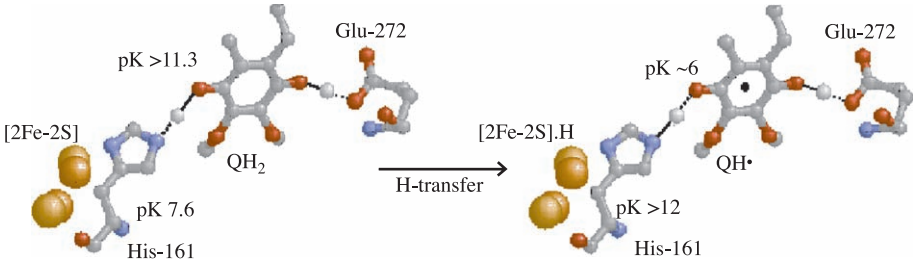

Fig. 2. A plausible model for the ES-complex, and of the EP-complex immediately after transfer of the first electron and proton (H-transfer). The structure of the stigmatellin-containing complex (PDB# 2bcc) was used to model binding of ubihydroquinone in the site with the same liganding as the stigmatellin. The coordinate data for the inhibitor were removed from the file to leave a vacant site. With the protein frozen, a ubiquinone (coordinates from the bacterial reaction center, PDB# 4rcr) was steered into position in the vacant Q_o-site using SCULPT V. 2.5 (Interactive Simulations Inc., San Diego, CA). The quinone was anchored artificially to N_ε of His-161 of the ISP, and to the nearest O-atom of the carboxylate group of Glu-272 of cyt b. Energy minimization with the quinone free to move allowed the structure to achieve a low energy configuration in the distal end of the Q_o-site that overlapped the volume occupied by stigmatellin. The protein was then freed, and structure within 15 Å of the quinone was allowed to relax using energy minimization. Finally, the constraints on the quinone were removed, and the structure was allowed to equilibrate for several hours. H-atoms were introduced into the PDB file positioned halfway between the donor and acceptor atoms to mimic a hydroquinone.

electron transfer over the pH range below the pK_1 at 7.6 could be naturally explained in terms of simple enzyme kinetics—the rate varied with [S] and approached saturation [23] (see below for further discussion)—and no stimulation over the high pH range was expected.

1.2. The binding constants involved in formation of the ES-complex

A long history from several labs of work in photosynthetic bacteria had shown that QH_2 is preferentially bound compared to Q on oxidation at the Q_o-site, so that the dependence of rate on E_h is displaced from the E_m of the pool (at ~90 mV) to an apparent E_m ~130–140 mV (reviewed in Ref. [9]). The molecular basis for this displacement was not understood. Similarly, it had previously been observed, as noted above, that the steady-state rate of QH_2 oxidation observed using isolated mitochondrial complexes showed a pH dependence over the range 5.5–9.5 [44,45]. This behavior was discussed in terms of two dissociable groups, the protonation state of which determined activity—the stimulation over the range <pH 8.0 was attributed to the need to deprotonate a group with pK ~6.5, and the loss of rate at pH 8.0 was attributed to the need for a protonated group with pK ~9. A more complete description in terms of 3 dissociable groups, with values pK ~5.7, 7.5 and 9.2 has recently been suggested [46]. However, the groups involved in control of rate had not been identified, and both Brandt and Okun [44] and Covián and Moreno-Sánchez [46] had excluded the involvement of the group giving rise to the pK_1 at ~7.6 of ISP_{ox} as the determinant for the stimulation in the range pH <8.

The rate of QH_2 oxidation in the first turnover of the site, seen in pre-steady-state kinetic measurements of the *Rhodobacter sphaeroides* bc_1 complex in situ, showed a similar pH dependence, with the stimulation over the range 5.5–8.0 titrating in with an apparent pK of ~6.3 [21,23,36–39]. This value was displaced from the pK of 7.6 expected to determine the concentration of the dissociated ISP_{ox} (with the imidazolate form of His-161) proposed as the form involved in formation of the ES-complex. At first sight this appeared to be contrary to the mechanism proposed. However, Crofts et al. [38] suggested a straightforward explanation for both displacements (that of $E_{m,\ Q/QH_2}$ and of pK_{ISP})—that they both reflect the same process—formation of the ES-complex of Fig. 2, as shown in Scheme 2. The equilibria involved in formation of the ES-complex are pulled over by the binding process through mass action—the binding of QH_2 would raise the apparent E_m for the oxidation reaction, and the binding of ISP_{ox} will pull the dissociated form of ISP_{ox} out of solution, giving an apparent shift in the pK—as shown by the equations in Scheme 2. Although not explicitly spelled out at the time [38], this conclusion was based on the fact that kinetic assays measured the concentration of the right-hand term (the ES-complex) in both equations. The rate is proportional to [ES]

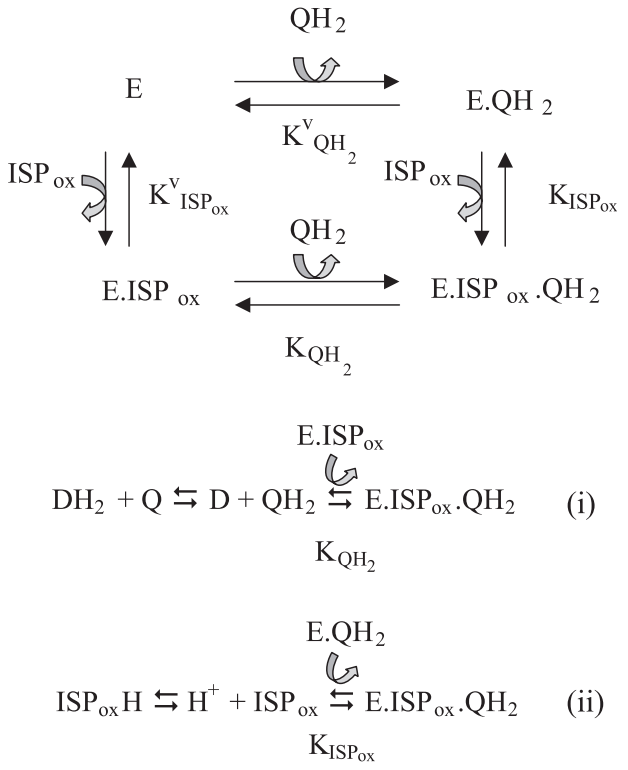

Scheme 2. Binding square involved in formation of the ES-complex, shown as a thermodynamic cycle with substrates and binding constants as discussed in the text. The equations below show the processes by which the thermodynamic parameters (E_m Q/QH_2 and p$K_{ISP_{ox}}$) are displaced by the binding reactions. In Eq. (i), DH_2 is an arbitrary electron donor whose contribution cancels in calculations (see text), best thought of as representing a reference electrode. The reactions shown here are simplified by omission of other processes involving the binding of ISP, Q and QH_2, since they are not relevant to the immediate argument. The binding constants for Q and QH_2 in the equilibrium state before oxidation of ISPH are similar [52] so that the E_m value for the bound couple is within experimental error the same as that for the free pool. The poise of overall reaction is measured through [ES], assayed kinetically under conditions in which all ISPH has been converted to ISP_{ox}. This simplifies the system by eliminating terms involving ISPH, but still leaves some ambiguity in description. A complete treatment would be somewhat intractable. The essential elements are brought out here by focusing on the formation of the ES-complex. However, the limitations inherent in measuring the poise of the bound couple through [ES], and our incomplete knowledge of binding constants for all components, necessarily mean that the values are approximations. For further discussion see The strength of the bond involved in formation of the gx = 1.80 complex, and [18–21].

through the standard kinetic equation, $v = k_{cat}$[ES]. The apparent E_m and pK values came from measurements of variation in rate (and hence [ES]) as a function of redox poise or pH. When the rate was measured at constant pH, and E_h was varied over the range of reduction of the Q pool, [QH_2] varied with constant [ISP_{ox}]; when pH was varied [ISP_{ox}] changed, and the E_h was adjusted so that the [QH_2] remained constant at the same near-saturating value. Consideration of the free-energy values for the partial processes of reaction Eqs. (i) and (ii) in Scheme 2 gives the following expressions. For Eq. (i), we first separate out the partial processes.

Reduction of the quinone pool with reference to the D/DH_2 couple,

$$DH_2 + Q \leftrightarrows D + QH_2$$

for which

$$\Delta G^o = -zF\Delta E^o = -zF(E_m^{freeQ-} - E_m^D)$$

and binding of QH_2 to form the ES-complex,

$$QH_2 + E.ISP_{ox} \leftrightarrows E.ISP_{ox}QH_2$$

for which

$$\Delta G^o = -RT\ln K_{QH_2}$$

Adding these equations gives us the reduction of the bound QH_2 with reference to the D/DH_2 couple and the free Q.

$$DH_2 + Q + E.ISP_{ox} \leftrightarrows D + E.ISP_{ox}QH_2$$

for which

$$\Delta G^o_{overall} = -zF(E_m^{ES} - E_m^D)$$

Since summing the ΔG values for the partial reactions also gives $\Delta G^o_{overall}$

$$\Delta G^o_{overall} = -zF(E_m^{free\ Q} - E_m^D) - RT\ln K_{QH_2}$$

from which we obtain

$$K_{QH_2} = \exp\left\{\frac{zF}{RT}\Delta E_m^{ES-free}\right\}$$

Similarly, for Eq. (ii)

$$\Delta G^o_{overall} = \Delta G^{ISP\ free}_{diss\ ox} + \Delta G^o_{blinding} = 2.303RT \cdot pK^{ISP^{bound}_{ox}}$$
$$= 2.303RT \cdot pK^{ISP^{free}_{ox}} - RT\ln K_{ISP_{ox}}$$

from which

$$K_{ISP_{ox}} = 10^{\Delta pK^{free-bound}}$$

In order to obtain a value for K_{QH_2}, we have to first justify the use of our kinetic determination of [ES] as appropriate to measurement of the mid-point of the half-cell implied in the overall reaction of Eq. (i), for which $E' = E_m + \frac{RT}{zF}\ln\frac{[EISP_{ox}.QH_2]}{[Q][E.ISP_{ox}]}$. We also have to reconcile this with the conventional expression relating ΔE_m to the binding constants for both QH_2 and Q, $\frac{K_{QH_2}}{K_Q} = \exp\left\{\frac{zF}{RT}\Delta E_m^{bound-free}\right\}$, which has a similar form to the expression above, but assumes a different half-cell for the bound states, for which $E' = E_m + \frac{RT}{zF}\ln\frac{[EISP_{ox}.QH_2]}{[E.ISP_{ox}Q]}$. The difference between the two expressions is the equation for the equilibrium constant for binding of Q—the binding of Q is assumed not to contribute a significant energy term in the first approach, so that $\Delta G^o_Q \sim 0$, and $K_Q \sim 1$. Because the ligand is in substantial excess (the Q-pool is in >30-fold excess over the bc_1 complex), the predominant oxidized form of the enzyme will be that with Q bound, and a value for $K_Q \sim 1$ is appropriate in both cases. Using this value, the two half-cell reactions, and the two expressions for K_{QH_2}, become equivalent.

With this approximation, the thermodynamic displacements measured kinetically ($\Delta E_m^{bound-free} \sim 40$ mV, and $\Delta pK^{free-bound} \sim 1.3$, [38]) can be converted to equilibrium constants using the relationships above, and give values of $K_{QH_2} \sim 21$ and $K_{ISP_{ox}} \sim 20$. Values in the literature for the displacements give a range of 17 ± 4 for these values, but within this error, both sets of data showed similar values for the equilibrium constant determining the displacement. These values provide two of the four equilibrium constants for the thermodynamic cycle represented by the binding square of reactions of Scheme 2. This binding square is the same as the set of equilibria on the left of Scheme 1 leading to formation of the ES-complex. Estimates of values for the other two missing terms ($K^v_{QH_2}$ and $K^v_{ISP_{ox}}$, for binding to the vacant enzyme) are available, both with uncertain values in the range 1 ± 1.5 [16,19,20]. The similarity of the two values derived from the displacements measured kinetically provide support for our suggestion that both reflect the same phenomenon—the liganding between QH_2 and ISP_{ox} involved in formation of the ES-complex—and suggest that the other two terms are of nearly equal value.

The equilibrium constants discussed above are derived from thermodynamic values, and are therefore formally dimensionless. The equivalent kinetic equilibrium constants will have the same value, but with dimensions to account for the concentration of the binding species[1]. For QH_2 this would reflect the concentration in the lipid phase, but for the ISP_{ox}, which is a tethered substrate in which the sum of concentration of all forms is equal to [bc_1 complex], a conventional concentration term is inappropriate. A formalism for treatment of this special case in the context of the binding constants involved in formation of the $g_x = 1.80$ complex was suggested by Shinkarev et al. [47], as discussed further below.

If the displacement of the pK observed kinetically does represent the binding constant involved in formation of the ES-complex, then the pH dependence over the range 5.5–8.0 is accounted for by the properties of the ISP without invoking a controlling effect of another dissociable group (cf. Ref. [46]). The configuration of the ES-complex suggested requires specific properties of the histidine side chain involved—it has to be the group responsible for the pK_1 measured from redox titration as a function of pH. This assignment now seems well justified [48–50]. The interpretation of a controlling role for this pK in determining the occupancy of the ES-complex is strongly supported by experiments with a mutant strain, Y156W, in which both the pK, and the whole curve for pH dependence, were shifted up by ~ 1 pH unit [37].

1.3. Role of Glu-272

An interesting conformational change of a buried glutamate side chain (Glu-272) was revealed in Berry's [16,20] structure PDB# 2bcc. In the presence of stigmatellin, Glu-272 had rotated 120° away from a position seen in the native complex (PDB# 1bcc), where it pointed towards heme b_L [1], to provide a second ligand to the inhibitor through H-bonding to a −OH group across the chromone ring structure of stigmatellin from the −C=O involved in interaction with the ISP. Molecular dynamics simulations [17] had predicted a relatively stable water chain leading from the aqueous phase on the cyt *c* side into the protein along the b_L heme edge to the Q_o-pocket. In the native structure, or that with myxothiazol bound, the Glu-272 carboxylate contacted this water chain. We suggested that the two ligands that bind stigmatellin were also involved in formation of the dual ES-complex, and that a movement of Glu-272 between these positions, with protonation after formation of the SQ intermediate, could provide a plausible pathway for transfer of a second proton from the site of oxidation of QH·[16]. Consistent with this, mutant strains with the equivalent glutamate in *Rb. sphaeroides* (E295) modified to aspartate, glycine or glutamine, showed small increases (1.5–2.5-fold) in apparent K_m for QH_2, lowered rates of electron transfer, and resistance to stigmatellin. The water chain we predicted has now been found in higher resolution structures from Hunte et al. [7,33], and these authors arrived at similar mechanistic conclusions. The water chain is also seen in a recent 2.1 Å structure of the bovine complex (PDB# 1pp9, Berry, E.A., by personal communication). The contribution of the H-bond from Glu-272 (Glu-295 in *Rb. sphaeroides* sequence) to the binding of QH_2 is likely in the range <1 kJ mol^{-1}, as judged from the small increase in K_m for QH_2 in mutant strains [16].

The mechanism proposed implies an important role in catalysis for this residue. The glutamate is completely conserved in α-proteobacteria and mitochondria, and also in cyanobacteria and chloroplasts [20,22], but variations are seen outside these groups. In *Rb. sphaeroides*, mutation slowed the rate substantially, but did not prevent turnover or photosynthetic growth under anaerobic conditions where the bc_1 complex activity is required [16]. Both these observation indicate that a glutamate at this position is not essential for function. However, data show a relatively weak contribution to the binding, and the structures show water molecules within the Q_o-pocket that form H-bonds with the carboxyl group O-atoms. Of the three mutants, E295Q showed the most dramatic inhibition. It seems possible therefore that on shortening the side chain (in the E295D strain), or replacement with a small side chain (in E295G), additional waters could enter the pocket, and facilitated the exit of the second proton. This option would be more constrained in the strongly inhibited E295Q mutant. Additional mutations at this site, in a His-tagged background to facilitate protein purification for spectroscopic work, are currently under study.

1.4. The g_x=1.800 complex

The $g_x = 1.80$ line in the CW X-band EPR spectrum of ISP is observed only when the quinone pool is oxidized

[1] The kinetic binding constants involving QH_2 and Q will have dimensions M^{-1}, referred to the lipid phase, where the Q-pool is 30–60 mM. Several different approaches can be taken to reconciling the values reported here with conventional values for the binding constants.

1. If K_Q is included in the equation relating K_{QH_2} to the observed displacement of E_m, the units cancel, and the value given for $\Delta G^{o}_{overall}$ derives from a dimensionless ratio representing the preferential binding of QH_2 over Q. By setting K_Q=1 (and ignoring the concentration term), we implicitly recognize the possibility that the value given here for K_{QH_2} represents a ratio of binding constants, so that the value for $\Delta G^{o}_{overall}$ is the free-energy change arising from the change in state rather than an absolute measure of the binding free-energy. However, because the change in state leading to formation of the ES complex involves the conversion of E.ISPH to $E.ISP_{OX}$, and the ISP can be at either the *b* or *c* interface, a full treatment would require consideration of the differential binding of Q and QH_2 to all these species.
2. The concentration ratios in the logarithmic terms of thermodynamic equations, and the related equilibrium constants, are dimensionless. Formally, this is achieved by division of all concentration terms by the activities in the standard state (1 M). However, when kinetic assay are used, the concentration of [ES] is in relative units of fractional occupancy, and this implies that actual concentrations are normalized to $[E_{tot}]$. The same normalization has to be applied to all terms with concentration units. Since the $[E_{tot}]$ of the bc_1 complex in the membrane is in the range 0.5–1 mM [9], equilibrium constants expressed in conventional M units will have values greater (for association constants) than the thermodynamic values by $1/[E_{tot}]$, or $1–2\times10^3$. The value for K_Q of 1 used here then becomes $1–2\times10^3$ M^{-1}, in the same range as the value estimated by Ding et al. [53] from the dependence on [Q] of the amplitude of the g_x=1.80 line of the EPR signal of ISPH (from $K_D \leq 1.6$ mM, $K_Q \geq 625$ M^{-1}, but this value is for binding of Q to the bc_1 complex with ISP reduced). Using this same adjustment, $K_{QH2} \sim 20{,}000$ M^{-1}.
3. An absolute value for K_{QH_2} can also in principle be obtained via the Michaelis–Menten relationship, since $K_M \sim 1/K_S^{assoc}$. The apparent K_m has been measured in the range 3–9 mM, depending on the relative concentration of Q_{total}/RC, and estimates of the membrane concentration of RC. From this apparent K_M, a value for $K_{QH_2} \sim 200$ M^{-1} might seem reasonable. However, this estimate ignores competition with Q and is clearly a lower limit. Substitution into the standard equation for a reversible competitive inhibitor gives

$$v_0 = \frac{V_{max}[QH_2]}{\frac{1}{K_{QH_2}} + [Q]\frac{K_Q}{K_{QH_2}} + [QH_2]}.$$

From this, at

$$v_0 = 1 \Big/ 2V_{max}, \frac{1}{K_{QH_2}} + [Q]\frac{K_Q}{K_{QH_2}} = [QH_2] = K_M^{app},$$

allowing calculation of K_{QH_2} from the experimental value of the apparent K_M. However, substitution into this equation involves estimation of ratios for both K_Q/K_{QH_2}, and $[QH_2]/[Q]$, and both are derived from the same experimental curve, that giving the apparent E_m at ~125 mV for ES. As a consequence, these terms cancel and give a value for K_{QH_2} of infinity.

and ISP reduced [51]. By analogy with quinone binding in the reaction center, several groups had speculated that the line-shape change at g_x might reflect a H-bond between Q and the side-chain of a histidine ligand to the [2Fe–2S] cluster of the reduced ISP [48,52], and formation of a similar bond involving QH_2 was an important component of reaction schemes from Ding et al. [52–54], Brandt and Okun [44], and Link [45,48]. This speculation was put on firmer ground when the structure of the extrinsic head domain was published, showing the liganding histidines exposed [55]. Ding et al. [52–54] had suggested that the tightly binding quinone at the Q_o-site (the Q_{os} species) of their double-occupancy model was stabilized by strong binding of a quinone by the ISPH through a histidine ligand. When the complete structure of the bc_1 complex was available [1], and the role of mobility of the ISP head became apparent, we suggested that the quinone species interacting with ISPH must represent a weakly bound H-bonded complex [16,19,20]. Preference for a weak binding was predicated on the need for rapid dissociation of the mobile head domain to allow participation in catalysis [19–21]. Structures in which stigmatellin was bound at the Q_o-site [1,7] showed an H-bond between a ring −C=O group of the chromone ring and His-161 of ISP, strongly suggesting that a similar bond between the quinone −C=O and His-161 might be responsible for the interaction revealed by the $g_x = 1.80$ line [19,20]. In order to explore the structure in greater detail, we collaborated with Dr. Sergei Dikanov and Dr. Rimma Samoilova in use of pulsed EPR to look at the [2Fe–2S] cluster ligands. We were able to show that the $g_x = 1.80$ complex involved a liganding N-atom (tentatively identified as N_δ of His-161) with structural characteristics (as determined from the spin interaction) similar to those seen in the stigmatellin complex [56]. The involvement of N_ε of the histidine ring in an H-bond with the occupant likely changed the spin interaction of the $^{14}N_\delta$ liganding the Fe with the paramagnetic cluster. The electron spin echo envelope modulation spectroscopy (ESEEM) spectra of both these bound forms differed from that seen in the presence of myxothiazol, where the liganding histidines are exposed to the aqueous phase. This conclusion supported the view that the H-bonded configuration of quinone and stigmatellin were similar, and represented the first direct structural information about occupancy of the Q_o-site by a quinone species. The Q.ISPH complex is formally an EP-complex, and the strength of this bond is therefore a parameter of thermodynamic interest in defining the energy landscape (see later).

1.5. The strength of the bond involved in formation of the g_x=1.80 complex

A substantial literature on the change of E_m of the ISP in the presence of inhibitors such as 5-undecyl-6-hydroxy-4,7-dioxobenzothiazol (UHDBT) and stigmatellin has been interpreted in terms of a preferential binding of the reduced ISP by the inhibitor [57,58]. Since the ESEEM data had shown that a similar bond is involved [56], the binding of ISPH by quinone might also be expected to induce an increase in $E_{m,\ ISP}$. We demonstrated this effect by looking at the change in kinetics of cyt *c* on flash activation of chromatophores with and without addition of myxothiazol, over the E_h range around the E_m of ISP. Quantification of the changes showed that the E_m in the presence of myxothiazol was ~40 mV lower than that in the absence of inhibitor [47,59]. Sharp et al. [60] had earlier reported a similar shift in E_m in the presence of MOA-stilbene measured directly by redox titration, and Darrouzet et al. [61] had independently investigated changes in $E_{m,\ ISP}$ in mutant strains with modified linker regions, and reported that myxothiazol induced a downward shift in the $E_{m,\ ISP}$, which in wild-type was ~40 mV, comparable to the value found from kinetics. From the structural data, no ligand is formed between myxothiazol and the ISP—rather the extrinsic domain was rotated away from its binding site on cyt *b* to expose the histidine ligands to the aqueous phase [5,20,62]. We suggested that the E_m measured in the presence of myxothiazol therefore likely reflected the unliganded state, and that the change in E_m induced by addition of inhibitor was due to displacement of Q by the inhibitor, leading to loss of the bound state seen in the $g_x = 1.80$ complex. From the E_m change, a binding constant of ~4 could be calculated, showing that a substantial fraction of the ISP_{red} would be bound at $E_{h,\ 7}$ ~200 mV [47].

Changes in E_m induced by inhibitors have previously been discussed in terms of a differential binding of a ligand (for example an inhibitor or a catalytic site) to oxidized and reduced forms of the redox couple (ISP_{ox}/ISPH, or Q/QH_2), through a formalism suggested by Clark [63]. This approach was introduced to describe changes in E_m on ligand binding in soluble systems, and the expression commonly used has the form $E_m^{app} = E_m^{free} + \frac{RT}{zF} \ln \frac{K_o^{dissoc}}{K_r^{dissoc}}$. However, it is not often recognized that this form is appropriate only if the ligand is in excess ([L]>K_o and [L]>K_r), so that the bound forms dominate the reaction mixture.

Use of this expression has provided valuable mechanistic insights, but the expression is inappropriate when a ligand binds much more strongly to one redox form than the other, unless the ligand is in excess. It is also inappropriate when discussing the unusual features associated with binding of a tethered substrate like the ISP, since the concentration terms have to be replaced by probability terms. Shinkarev et al. [47] developed a different expression that made it possible to avoid these difficulties, with $E_m^{app} = E_m^{free} + \frac{RT}{zF} \ln \frac{1+K_r^{assoc}}{1+K_o^{assoc}}$. When both K_o and K_r are large compared to 1 (strong binding to both forms), this expression approaches that of Clark. However, when one form binds weakly and the other strongly, as is likely the case for interaction of ISPH with QH_2

and Q, respectively, one term in the ratio will approach 1, and the other K. In this case the E_m change provides a measure of the binding constant for the stronger binding form—in this instance, Q. Space does not permit discussion of the limitations of this useful approach, for which the reader should consult the original [47].

The binding constant for formation of the $g_x = 1.80$ complex calculated using this formalism, $K_{assoc} \sim 4$, was in the same range as that expected for the binding of QH_2 by Glu-272, as seen from the increased K_m in mutant strains ($K_m^G/K_m^E \sim 2.3$) [47]. Since the first of these values refers to binding of Q to the Q_o-site with ISPH, and the second refers to the fraction of binding of QH_2 not attributable to interaction with ISPH, they can be thought of as differential binding constants for interaction of Q and QH_2 with the enzyme under the conditions expected in a redox titration. The similar values explain why the apparent E_m for formation of the $g_x = 1.80$ complex titrates with a value close to the mid-point of the quinone pool [19].

1.6. The energy profile of the QH_2 oxidation reaction; identification of limiting steps

In the discussion on formation of the ES-complex above, it was proposed that the ES-complex is stabilized by formation of an H-bond between the −OH of QH_2 and the imidazolate ring of the dissociated ISP_{ox}. Electron transfer from QH_2 to ISP_{ox} would have to occur through this H-bond. This proposal has important consequences for the mechanism. Because the pK on the reduced form of ISP is >12, electron transfer would have to be coupled to H^+ transfer so that the reaction is formally an H-transfer. Release of the proton would occur on oxidation of ISPH by cyt c_1 (at pK>pK_1) or on rebinding of $ISP_{ox}H$ to form the ES-complex (at pH < pK_1).

As noted above, a second mechanistic consequence is that formation of the ES-complex does not involve dissociation of QH_2 to QH^-. Electron transfer can proceed from this state without the prior need for release of a proton implicit in the "proton-gated charge transfer" mechanism [43,44]. This proposal solves an obvious embarrassment inherent in mechanisms with QH^- as a necessary intermediate—that the pH dependence of electron transfer for the bc_1 complex in the higher pH range was the opposite of that expected—a slowing of rate was seen rather than the acceleration seen in the Rich and Bendall [41] experiments. Despite this difficulty, Brandt and Okun [44] justified their mechanism by invoking two separate contributions—the two pK values affecting rate as discussed above—and a strong dependence on pH of the activation energy for steady-state electron transfer, but this does not reconcile the internal inconsistency, and the pH dependence of activation energy was contrary to our own findings.

The studies of Crofts and Wang [64] on the pre-steady-state kinetics of the complex in its native state, later extended to a wider range of conditions by Hong et al. [21], showed the following:

(a) The reaction with the slowest rate under conditions of substrate saturation was the oxidation of QH_2 from the ES-complex. This was also the reaction with the highest activation barrier.
(b) In contrast to the observation on steady-state electron transfer with the isolated mitochondrial complex [44], the activation barrier for oxidation of QH_2 in the pre-steady-state was *independent* of pH. This removed any justification for a mechanism involving a necessary dissociation of QH_2 to QH^- before electron transfer.
(c) The activation barrier was also independent of the redox poise of the quinone pool. From the discussion on formation of the ES-complex above, it will be clear that varying pH below the pK for ISP_{ox} varies the concentration of one substrate—the dissociated ISP_{ox} species active in formation of the ES-complex. Reduction of the quinone pool increases the concentration of QH_2, the other substrate. These independencies therefore showed that the activation barrier was independent of substrate concentration, and after formation of the ES-complex, as is the norm for enzyme reactions.
(d) As shown by acceleration of the rate of electron transfer over the lower pH range, and the acceleration on reduction of the pool, the rate varied with concentration of either substrate, as expected from simple Michaelis–Menten considerations.
(e) The dependence of rate on driving force for the first electron transfer, as determined from experiments taking advantage of changes in $E_{m,\ ISP}$ in mutant strains, identified this as the limiting partial process (see below).
(f) Reactions associated with movement of the ISP extrinsic domain were not limiting. The movement of the ISP could be assayed by measuring the lag times involved in reactions that incorporate it as a partial process. The time not accounted for by electron transfer events was always short (< 30 μs), and the reactions all had low activation barriers [21]. This was in line with weak association constants [19], and the simple constrained diffusion mechanism suggested by the structures and MD simulations [17].

1.7. Dependence of rate on driving force and on pH

Analysis of the kinetics in strains with mutations in ISP that lowered the E_m value had shown that the steady-state rate of QH_2 oxidation depended on the E_m, and therefore on the driving force for the first electron transfer [65–67], and we showed a similar dependence on driving force in pre-steady-state measurements assaying oxidation of the first QH_2 [37–39,68]. In contrast, the overall rate did not appear to be greatly modified by changes in E_m of heme b_L, either by mutation, or on prior reduction of heme b_H [21]. This

strongly suggested that transfer of the first electron (from QH_2 to ISP_{ox}) was the rate-limiting step.

With identification of the rate-limiting step, attention could be shifted to detailed consideration of the factors determining rate—distance, driving force and reorganization energy [69,70]. In the context of the proposed structure of the ES-complex, the rate observed in wild-type was much slower than that expected from our model. Assuming that electron transfer occurred through a H-bond between QH_2 and His-161 [16,21], the rate expected from the Moser et al. [69] De Vault [70] treatment, using the distance of ~ 7 Å suggested by the structure, and a conventional value for the reorganization energy ($\lambda \sim 0.75$ eV) was $\sim$ three orders of magnitude higher than the rate observed. Hong et al. [21] could explain the observed rate if a high value for reorganization energy ($\lambda \sim 2.0$ eV) was used, in line with the high activation barrier, but this value was much higher than that found in other electron transfer reactions occurring over similar distances [69], and no obvious feature of the structure could be used to justify such a high value. The problem then was to find a better explanation for this anomalously slow rate.

Our own work on the dependence of reaction rate on driving force used mutant strains with modifications in ISP at Tyr-156 (Tyr-165 in bovine sequence) [37]. This residue forms a H-bond from the tyrosine-OH to the Sγ of one of the cysteine ligands (Cys-139, bovine)—one of several H-bonds to the cluster contributing to the high E_m and low pK [49]. Measurement of the E_m and pK values of these strains showed that all had decreases in E_m—minor for the Y156H strain, but increasingly more substantial for strains Y156F, L, and W. However, for one strain (Y156W), in addition to the substantial decrease in E_m measured at pH 7, there was also a substantial increase in pK (from 7.6 to 8.5). The effect of change in E_m on the rate of reaction could be assessed by plotting the logarithm of the rate-constant for oxidation of QH_2 as a function of ΔE_m at pH 7.0. Assuming that the driving force was given by the value of ΔG^o for the overall reaction, and that the E_m of the acceptor was unchanged by mutations in ISP, ΔE_m is a direct measure of $\Delta\Delta G^o$. In such plots, the points followed the dependence of rate on driving force expected from Marcus theory (reviewed in Ref. [70]) (Fig. 3). However, a substantial part of the inhibition observed in strain Y156W (open square in Fig. 3) could be attributed to the effect of the pK change on the concentration of the dissociated form as substrate. At pH 7.0 and with a pK of 8.5, the concentration of ISP_{ox} would have been eight times lower than with a pK at 7.6, and the rate would have reflected this lower concentration. This affect of pK could be illustrated by plotting on the same scale the rate for strain Y156W measured at pH 8.0, with the ΔE_m adjusted to the value appropriate to this pH (open triangle in Fig. 3). The value then fell away from the slope defined by the other points [37]. This anomaly called into question the validity of using the Marcus explanation for the inhibitory effect observed, but provided an important clue as to how the anomalously slow rate could be explained.

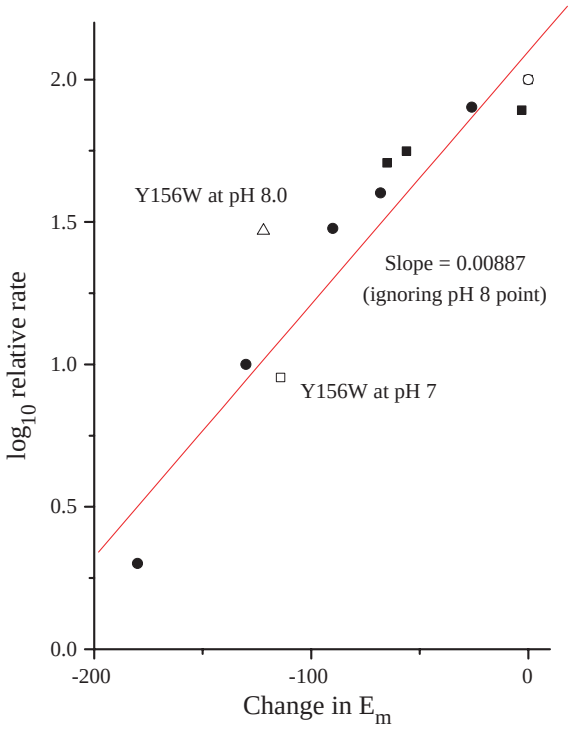

Fig. 3. The dependence of rate on driving force for electron transfer as determined in mutant strains with modified E_m, ISP. The points show data plotted on a $\log_{10}$ scale for the rate constants (or maximal rates under saturating conditions) of quinol oxidation by the bc_1 complex from bacteria or mitochondria from strains with mutations in the ISP that modify the E_m of the [2Fe–2S] cluster. The rates have been normalized to the rate in wild-type strains (taken as 100). The values are plotted against the change in E_m determined by redox titration compared to wild-type. Data shown as squares are from Ref. [37]; other values from Refs. [40,66,67]. For the data from our own work [37], experiments measured the rate of heme b_H reduction in the presence of antimycin in chromatophores from *Rb. sphaeroides*. The reactions of the bc_1 complex were initiated by a saturating flash of light to excite turnover of the photochemical reaction centers. The reaction generates the substrates for the bc_1 complex in <10 μs. All experiments were performed under anaerobic conditions at pH 7, and E_h 100 mV, under which conditions both substrates (ISP_{ox} and QH_2) were present ~ 200 μs after the flash at close to saturating concentration. The points indicated by the open symbols were obtained with strain Y156W. The open triangle indicates a point measured at pH 8, with the E_h adjusted to 30 mV so as to maintain the same degree of reduction of the pool as for the other points. Under these conditions both substrates were at close to saturating concentration for this strain. See text for further explanation. The slope shown is the best fit to points other than the open triangle; see text for explanation.

For an explanation of this anomalous behavior, we must look in greater detail at the role of pK_1 of ISP_{ox} in controlling several critical parameters:

(1) The E_m value of the ISP, together with the E_m of the SQ/QH_2 couple, determines the overall redox driving force for the first electron transfer, as summarized above and discussed extensively by Hong et al. [21] and in Ref. [37].
(2) In the formation of the ES-complex, the dissociated (imidazolate) form is the substrate (see above, and Refs.

[35,40]). The concentration of this form depends on pH, and on the pK of the group undergoing dissociation, assumed to be pK_1 due to dissociation of His-161.

(3) The pK_1 at 7.6 on the oxidized form results in a dependence of $E_{m,\ ISP}$ on pH—the value decreases above pH 7.0, with a ~59 mV/pH unit slope above the pK. A second pK (pK_2) on the oxidized form at 9.2 increases the slope at higher pH. Over this range (at pH>8), the overall rate, and the rate of the first electron transfer, both decrease. The decrease in E_m of ISP might be expected always to determine the overall driving force [46], but because the E_m of the Q/QH_2 couple also decreases by ~59 mV/pH, the driving force is constant with pH over the range of pK_1, and pK_2 will be the critical determinant for the change in driving force. This driving force effect, together with the effect on concentration (as in (2) above), provided an explanation for the entire dependence of rate on pH over the physiological range, in terms of the pK values of ISP_{ox}.

(4) The pK_1 also plays a critical role in determining the activation barrier, as discussed more extensively below.

As an aside from our consideration of the Q_o-site reaction, the equilibrium constant between cyt c_1 and ISP is also determined by pK_1 over the physiological range, because the E_m of cyt c_1 shows no pH dependence over this range. This has important consequences for the kinetics of the high potential chain measured in pre-steady-state experiments [27,71].

1.8. Proton-coupled electron transfer as a determinant in the rate-constant for QH_2 oxidation

Work on model compounds by Roberts et al. [72] had demonstrated the controlling effect of pK values on coupled H^+ and electron transfer through H-bonds in aprotic media. A detailed theoretical treatment by Cukier and Nocera [73] suggested that, for the case in which the proton transfer step was unfavorable, the rate was controlled by the low probability for a favorable configuration from which electron transfer could occur, and they developed a Marcus theory treatment in which the contributions of proton transfer and electron transfer were treated using separate terms for driving force but a common reorganization energy.

The quantum mechanical treatment required was complex, but the idea was essentially simple—electron transfer through an H-bond is determined by the probability of finding the H^+ in a suitable configuration in the bond.

Graige et al. [74], in discussion of the proton-coupled electron transfer reaction at the Q_B-site in photochemical reaction centers, had made simplifying assumptions that allowed separation of the role of the proton transfer from the electron transfer, by treating the former through a probability function. Combining these approaches has led us to propose a treatment of the dependence of rate on driving force as applied to the Q_o-site reaction [39], which avoids the difficulties arising from quantum mechanical considerations of the role of the proton [73]:

(i) The electron transfer can occur only when the proton configuration is favorable. This requires that the proton be transferred through the H-bond before electron transfer can occur.

$$E.b_L.QH_2ISP_{ox} \overset{\Delta G_{proton}}{\leftrightarrows} E.b_L.QH^-.H^+ISP_{ox} \overset{\Delta G^{\ddagger}_{electron}}{\leftrightarrows} ES^{\ddagger} \rightarrow E.b_L.QH \cdot .ISPH \quad (1)$$

(ii) The value for ΔG_{proton} is given by the Brønsted relationship [75], which describes the equilibrium distribution of the H^+ along a H-bond in terms of the pK values of the H-bond donor (pK_D) and acceptor (pK_A):

$$\Delta G_{proton} = 2.303RT(pK_D - pK_A) = 2.303RT(pK_{QH_2} - pK_{ISP_{ox}})$$

(iii) The occupancy of the proton-transfer state needed for electron transfer is determined by Brønsted term, as above. Given the pK values for QH_2 (pK >11.5) and ISP_{ox} (pK ~7.6), the configuration is thermodynamically highly unfavorable, and the low probability of accessing the state represents a substantial part of the activation barrier. This probability term recalls the explanation of Rich and Bendall [41] for the pH dependence of QH_2 oxidation. In both cases, the unfavorable state is determined by the high pK of the donor (QH_2). However, while in the solution experiment, or in the "proton-gated charge-transfer" mechanism [44], the pK determines the probability of dissociation to the quinol anion, in the present case it determines, relative to the pK of the acceptor, the distribution of the H^+ along the H-bond. The step represented by $\{ES\}^{\#}$ in Scheme 1 is replaced by the two partial processes shown in Eq. (1). In terms of an Arrhenius representation, this gives:

$$k_{lim} = k_o\exp\{-(\Delta G^{\ddagger}_{electron} + \Delta G_{proton})F/RT)\} = \{k_o\exp - \Delta G^{\ddagger}_{electron}F/RT)\}\exp\{-2.303\Delta pK\} \quad (2)$$

(iv) The reaction occurs at a protein interface that appears from the structures to be aprotic and anhydrous, so it is unlikely that the proton will equilibrate with the aqueous phase [7,33,39].

(v) Rates of H^+ transfer through H-bonds are inherently rapid (~2×10^{11} s^{-1}), ~1000 faster than the maximal electron transfer rate at this distance [75,76]. To a close approximation, the proton transfer contribution can therefore be treated as a separate

probability function given by the Brønsted term. This allows for a great simplification in thermodynamic treatment. It will be recognized that the reaction sequence of Eq. (1), with the parameters for equilibrium and rate constants discussed above, represents one of the classes of electron transfer reactions involving kinetic complexity discussed by Davidson [77]. The overall electron transfer is *coupled* to the proton transfer step, which has a low probability, but rapid rates for the reactions by which the intermediate step is equilibrated, compared to the electron transfer step. As discussed by Davidson [77], the overall rate constant for such processes is given by

$$k_{\mathrm{lim}} = K_x k_{\mathrm{ET}} \tag{3}$$

where K_x is the equilibrium constant for establishing the intermediate state, and k_{ET} is the rate constant for the electron transfer step. This is an alternative representation of Eq. (2).

(vi) Using the pre-exponential terms suggested by Moser et al. [69], a Marcus expression for the electron transfer energy barrier, and the Brønsted term for the proton barrier, the following equation for the rate constant was proposed [39]. This is equivalent to Eq. (2) written in $\log_{10}$ form, with the two ΔG terms and k_o expanded.

$$\log_{10}k_{\mathrm{lim}} = 13 - \frac{\beta}{2.303}(R-3.6) - \gamma\frac{(\Delta G^{\circ}_{e}+\lambda)^2}{\lambda} - (\mathrm{p}K_{\mathrm{QH_2}} - \mathrm{p}K_{\mathrm{ISP_{ox}}}) \tag{4}$$

Here β is 1.4, the slope of the Moser–Dutton relationship between $\log_{10}k$ and distance, R is the distance in angstroms, ΔG°_{e} is the driving force for the electron transfer step, and λ is the reorganization energy (both in electrical units). The term γ has a value of 3.1 following the Moser et al. [69] treatment for the electron transfer step adopted in the previous paper [39].

This equation has been incorporated into a simple computer model that provides a framework for testing the effects of changes in critical parameters [21]. The current version includes routines to allow exploration of the contribution of the Brønsted term. The program also allows a choice between the Moser–Dutton factor of 3.1 for γ in Eq. (4), which includes quantum mechanical contributions from tunneling [69,70], or a classical Marcus term ($F/(4\times 2.303\,RT)$ [70,78]), which has a value of $\sim$ 4.2 at 298 K. In the program, the curve of $\log_{10}k_{\mathrm{lim}}$ vs. ΔG is plotted using values input by the user for the critical parameters γ, R, λ, and the two pKs. These make it possible to move the curve around the plot area so as to match experimental values for k and reaction driving force (ΔG°_{e}). The program keeps track of the First Law interdependence of thermodynamic parameters for partitioning of the activation barrier, and those for transfer of the first and second electrons based on the nature of the bifurcated reaction, as detailed in Ref. [21].

This program has been used to analyze the experimental data summarized in Fig. 3, in which E_{m} and pK values were varied by mutagenesis. The data shown in Fig. 3 include values from our own work [37] and some from the literature for comparison [40,65–67], scaled to the rate in wild-type strains. The plot of $\log_{10}(k)$ against change in driving force (given by the change in E_{m} in the mutant strains) shows that the rate varied with driving force in a manner consistent with Marcus theory [21,37,40,65–67]. However, as noted above, the results using strain Y156W (with pK_1 $\sim$ 8.5) showed anomalous properties [37].

With the insight provided by the treatment above, a plausible explanation for this behavior can be offered. The inhibition of rate because of the higher $\mathrm{p}K_{\mathrm{ISP_{ox}}}$ (which reduces the substrate concentration) is counteracted by a stimulation due to a higher probability of favorable proton configuration arising from the contribution of the higher $\mathrm{p}K_{\mathrm{ISP_{ox}}}$ to the Brønsted term.

The critical points can best be explained in terms of Marcus curves generated by the program (Fig. 4). The parameters were adjusted to take account of the observed rate constant ($k_{\mathrm{cat}} \sim 1.5\times 10^3$ s^{-1}) and activation barrier ($\sim$ 65 kJ mol^{-1}) for the first electron transfer in the wild-type [21], the E_{m} values of the reactants and products (and hence $\Delta G^{\circ\prime}$ for the overall reaction), pK values, and the distance of 6–7 Å over which the first electron transfer must occur if our model for the ES-complex is correct.

Before examining the curves, it is worth noting some properties of the equation and the resulting curves. The inverted parabola has a width determined by γ (the lower value resulting from the Moser et al. [69] treatment gives a wider parabola, and consequently a shallower slope at any particular value for $\log_{10}k$), and by λ (larger values give wider parabolas), and is offset vertically by changing the distance, R, and Brønsted terms (pK values). These latter do not modify the shape of the curve since their value in the equation is independent of ΔG, the dependent variable. Changing λ also shifts the curve horizontally so that the peak position (when $\lambda = -\Delta G$) is at higher values of ΔG for lower values of λ. In Fig. 4, a limited area of the plot is highlighted. To avoid confusion in looking at the positions of the curves, it is worth noting that a vertical shift in the position of the parabola will appear as a horizontal displacement of the curve, which should not be confused with the horizontal displacement due to a change in λ.

We are interested in explaining the dependence of an electron transfer reaction on redox driving force. Although the overall reaction requires both electron transfer steps, and is exergonic, we focus here in the first electron transfer reaction, because that is rate-determining. In the discussion here, the overall driving force for the first electron transfer is endergonic, but this is not essential to the treatment. A

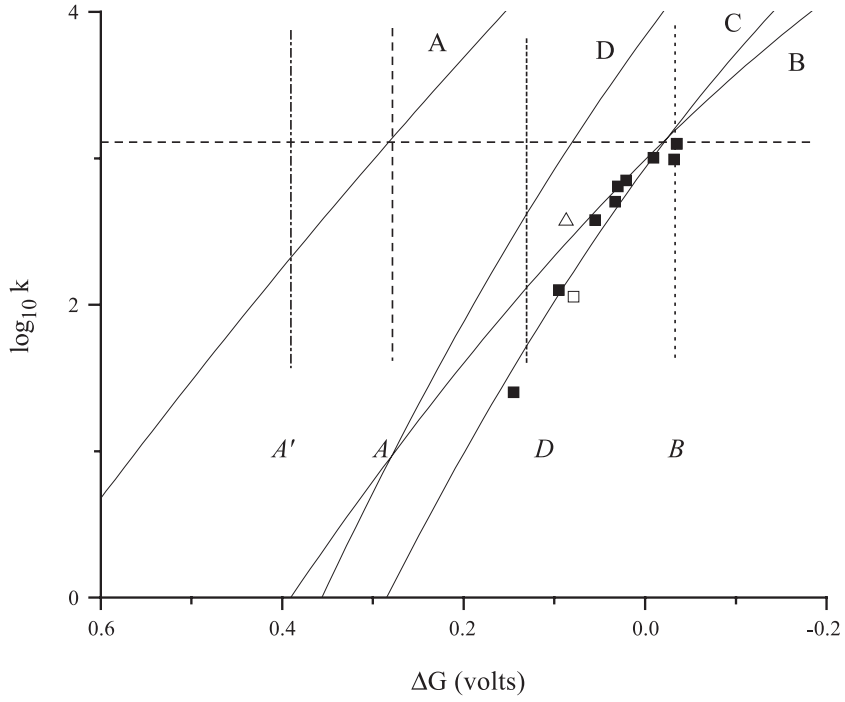

Fig. 4. Marcus curves showing the variation in rate with driving force for different conditions discussed in the text. Default parameters used in all curves were: $R_1 = 7$ Å, $E_{m,\ b_L} = -90$ mV, $E_{m,\ Q/QH_2\ (pool)} = 90$, $E_{m,\ Q/QH_2\ (bound)} = 130$, $E_{m,\ Q/QH^{\cdot}} = -325$, $E_{m,\ QH./QH_2} = 585$, $E^{act} = 0.65$ V. Curve A—Parameters: $E_{m,\ ISP} = 310$ mV (or 198 mV for Y156W, line A'); $\Delta G_1^{overall} = \Delta G_1^e = 275$ mV (line A) (or $\Delta G_1^e = 387$ mV for Y156W, line A'), $\lambda_1 = 1.87$ V. Values returned: rate, first $e^- = k_{ET} = k_{cat} = 1.26 \times 10^3\ s^{-1}$, slope (at ΔG_1^e) $= -0.0071$/mV (intercept on line A) (or slope $= -0.0074$/mV for Y156W, intercept on line A'). Curve B—Parameters: $E_{m,ISP} = 310$ mV; $\Delta G_1^{overall} = 275$ mV, $\Delta G_1^e = -32$ mV, $pK_{ISP_{ox}} = 6.3$, $pK_{QH_2} = 11.5$; $\Delta G^{proton}/F = 307$ mV. Values returned: rate, first $e^- = k_{cat} = 1.51 \times 10^3$ $e^- = k_{cat} = 1.51 \times 10^3\ s^{-1}$, $k_{ET} = 2.4 \times 10^8\ s^{-1}$, $\lambda_1 = 0.84$ V, slope (at ΔG_1^e) $= -0.0059$/mV (intercept on line B). Curve C—Parameters: $E_{m,\ ISP} = 310$ mV; $\Delta G_1^{overall} = 275$ mV, $\Delta G_1^e = -32$ mV, $pK_{ISP_{ox}} = 6.3$, $pK_{QH_2} = 11.5$; $\Delta G^{proton}/F = 307$ mV. Values returned: rate, first $e^- = k_{cat} = 1.55 \times 10^3\ s^{-1}$, $k_{ET} = 2.45 \times 10^8\ s^{-1}$, $\lambda_1 = 0.66$ V, slope (at ΔG_1^e) $= -0.008$/mV (intercept on line B). Curve D—Parameters: $E_{m,\ ISP} = 198$ mV, $\lambda_1 = 0.66$ V, $\Delta G_1^{overall} = 387$ mV, $\Delta G_1^e = 133$ mV, $pK_{ISP_{ox}} = 7.2$, $pK_{QH_2} = 11.5$; $\Delta G^{proton}/F = 254$ mV. Values returned: rate, first $e^- = 3.41 \times 10^2\ s^{-1}$, $k_{ET} = 6.8 \times 10^6\ s^{-1}$, $\lambda_1 = 0.66$ $\lambda_1 = 0.66$ V, slope (at ΔG_1^e) $= -0.01$/mV (intercept on line D). For curve A, the driving force for the first electron transfer is the overall driving force given (in electrical units) by $\Delta G^{overall} = \Delta G^o/F = -\Delta E_m$, using values for $E_{m,\ ISP}$ and $E_{m,\ QH/QH_2}$ given above. For curves B, C and D, the driving force for the first electron transfer is ΔG_1^e, given by the difference between $\Delta G_1^{\ overall}$ and the Brønsted energy term, and is: $\Delta G_1^e = \Delta G^{overall} - \Delta G^{proton} = \Delta G^{overall} - 2.303\frac{RT}{F}(pK_D - pK_A)$. The points plotted are those from Fig. 3, scaled to the rate measured in *Rb. sphaeroides* as described in the text, and to a driving force assuming the parameters above for curve B or C. The open symbols show values for mutant strain Y156W.

conventional Marcus treatment is used, rather than the somewhat misleading version suggested as appropriate for the endergonic direction in Ref. [80]. The curve plotted is $\log_{10}k$ vs. ΔG for the electron transfer step, and is independent of the assignment of ΔG to a particular partial process. However, when it comes to finding a fit to the data, ΔG has an explicit meaning that is model-dependent, as explained below. In moving the curve around the plot area to fit the data, the parameters for the curve take on the explicit meaning for ΔG to match the meaning implicit in the vertical line at the driving force of a particular partial process.

Since $\log_{10}k$ and ΔG are the variables plotted, the unique values for k and driving force (ΔG^o) appropriate for a particular reaction are related to the curves through intercepts of the plotted curve with horizontal and vertical lines, respectively, at the values given by experimental data. Since the first electron transfer step is limiting, a satisfactory fit of the plotted curve to the experimental values is found when the three lines intercept at a single point.

The solid curves show the variation of $\log_{10}k_{cat}$ for electron transfer as a function of driving force, using either a Moser et al. [69], or a classical Marcus [70,78] treatment, or either of these modified by the Brønsted term, for a particular set of values for λ, R, γ, and pKs, as detailed in the figure legends. For the unmodified treatments, the driving force for the first electron was the $\Delta G^{overall}$. By splitting out the Brønsted term, we are assuming that changes in $E_{m,\ ISP}$ do not affect the proton distribution. For the plots modified by the Brønsted term, the redox driving force (changed by changes in $E_{m,\ ISP}$) was the fraction of the overall driving force not attributable to the Brønsted term. This is the value shown as ΔG_1^e in the figure legend, and by the vertical broken lines. The values for $\Delta G^{overall}$ were calculated from $E_{m,\ 7}$ values, using for E_m of ISP_{ox} either the value for the wild-type ($E_{m,\ 7} = 310$ mV) or that for mutant Y156W, in which the $E_{m,\ 7}$ was shifted to 198 mV. The acceptor E_m used was that for the SQ/QH_2 couple, with a value of 585 mV. This value was based on the case favored by Hong et al. [21] in which the

first electron transfer was uphill, with a positive value for ΔG^{o}. Justification for this assumption, which is in line with experimental observation, can be found in the earlier literature [21,64,79]. The horizontal dashed line is positioned at the observed value for $\log_{10}k_{cat}$ for wild-type; the many different lines appropriate for rates measured in mutant strains have been omitted for clarity. For any particular reaction, plausible parameters for the curve are those at which the parabola intercepts both the horizontal line for the measured $\log_{10}k$, and the vertical line for the appropriate driving force. To find this point, the parameters of the curve are adjusted till the intercept condition is fulfilled. Curves can be generated to fit other plausible scenarios for the first electron transfer [21] by choice of different values for $E_{m,\ SQ/QH_2}$ to modify $\Delta G^{overall}$. This will not affect the general shape of the curves generated, or the changes in position arising from changes in pK, but will determine the values needed to produce a suitable intercept of the curve with the experimental values.

In the evaluation of these curves, it should be noted that the rates discussed (except those for the open triangle) were from experiments in which kinetics were measured at $E_h \sim 100$ mV and at pH 7.0, conditions in which the concentrations for both substrates were close to saturation for wild-type (with E_m for ISP at 310 mV). The measured rates were therefore close to k_{cat}, and appropriate for comparison with the Marcus curves, for which it is assumed that the ES-complex was fully populated (saturating substrate concentrations).

Curve A is that given by the standard Moser et al. treatment assuming pure electron transfer, similar to that previously published [21]. The vertical dashed line A shows a driving force for the first electron transfer appropriate for wild-type ISP. Using the full distance from the >C=O oxygen of stigmatellin to the nearest Fe of the cluster, a value for $\lambda = 1.87$ eV was needed in order to get the rate low enough. This value for distance (7 Å) is at the high end for the O–Fe distance from different structures (which range from 6.68 to 7.1 Å). If the liganding histidine participates in the electronic structure of the cluster, the distance would be smaller; at 6.3 Å, the value for λ needed is the maximal value (2.01 V) compatible with the large activation barrier measured. All plausible values for λ are much higher than experimental values found for similar electron transfer reactions. The slope at the intercept point (~ -0.007/mV) is considerably less than that of the experimental curve of Fig. 3 (~ -0.009/mV).

The vertical dash-dot line A' shows the driving force assuming $E_{m,\ ISP} = 198$ mV, the value found at pH 7 in mutant Y156W. The intercept of the Moser–Dutton curve with this line is at a lower rate, showing the "inhibition" compared to the wild-type k_{cat}, which could be attributable to the change in driving force if everything else was equal.

Curve B is the Moser–Dutton curve, but incorporating the Brønsted term of Eq. (2). This places part of the activation barrier in the improbable proton transfer, so that the fraction to be accounted for in the electron transfer is smaller. The parabola is shifted down by $-(pK_{QH_2} - pK_{ISPox})$, which has the effect of shifting the intercept with the horizontal $\log_{10}k$ line to the right. Since a fraction of the driving force also comes from the Brønsted term, the driving force for the electron transfer step also has to be adjusted. This is shown by the vertical dotted line B, with a value appropriate for wild-type ISP. We have assumed here that the pK value appropriate to the calculation is that for the ES-complex (6.3 rather than 7.6 for the free form) leading to values for λ close to the expected range for the electron transfer step. The lower value of λ narrows the parabola, and shifts it to the left. The result of all these shifts is a slope of the curve at the intercept similar to that for curve A. However, the slope at the intercept (~ -0.006/mV) is still lower than the slope from experiment.

Curve C shows the profile using a classical Marcus term for the activation energy, but partitioning out the proton-transfer probability using the Brønsted term. The larger value for γ results in a narrower parabola and hence a steeper slope. Values for other parameters are similar to those for curve B, but the narrowing necessitates a small change in λ to move the curve over to give the same intercept. The steeper slope at the intercept is more in line with that from experimental values, as shown by the points plotted, taken from Fig. 3. The values for $\log_{10}k$ for these points are those for Fig. 3, scaled to k_{cat} for wild-type. The values for ΔG_1^e were adjusted as follows: the value of change in E_m shown in Fig. 3 was added to the value for E_m of the wild-type strain to restore the measured E_m, and this was then used, with the assumed value for $E_{m,\ SQ/QH_2}$ to calculate the overall driving force, $\Delta G^{overall}$. The driving force for the electron transfer step was then taken as the difference between this value and ΔG^{proton} given by the Brønsted term. This brings the values for the mutant strains into line with the value for ΔG_1^e for wild-type (vertical line B), as detailed in the figure legend.

Curve D shows the effect of using the same treatment as for curve C, but with the pK for ISP_{ox} appropriate for the Y156W strain. As for curves B and C, the value appropriate for the ES-complex (7.2 rather than 8.5 for the free form) was assumed. This offsets the curve vertically by the pK difference, and shifts the intercept with $\log_{10}k_{cat}$ to the left. Changing the pK also changes the contribution of the Brønsted term to $\Delta G^{overall}$, and therefore changes the driving force for the electron transfer step, from the value indicated by the open square (derived from the $E_{m,\ 7}$ value for Y156W) to that indicated by vertical line D. The intercept of curve D with line D shows the value for $\log_{10}k_{cat}$ expected for strain Y156W on the basis of the model. This maximal rate constant is close to the value measured at pH 8.0 (open triangle), conditions close to those for maximal rate for this strain [37]. The expected rate measured at pH 7.0 would be lower than k_{cat} because the concentration of the ISP_{ox} substrate will be lower by

$\sim \log_{10}\Delta pK$. This would give an apparent rate constant close to the measured rate at pH 7.0 represented by the open square.

The main points to be derived from this analysis are as follows:

1. By introducing the intermediate proton configuration, we can explain the otherwise anomalously slow first electron transfer. The transfer of the electron occurs with a high rate constant, but from a weakly populated state. The probability of occupancy of this state is given by the Brønsted term. The parameters for the electron transfer step (k_{ET} and λ) are in line with those in other systems operating over similar distances with similar driving forces.
2. Inclusion of the Brønsted term also provides an explanation for the otherwise anomalous behavior in strain Y156W. The change in pK with respect to wild-type leads to changes in rate measured at pH 7 in which a slowing due to the substrate effect is compensate by a speeding up due to the smaller value of the Brønsted term. Changes in pK are expected to have a number of more subtle effects on the profile of the activation barrier because of the interplay between the Brønsted term, $\Delta G^{overall}$, and the driving force for the electron transfer step. When all these effects are taken into account, the anomalous behavior of strain Y156W seems to be quite satisfactorily explained. This success provides strong support to the suggestion that proton-coupled electron transfer at the Q_o-site of the bc_1 complex controls the rate of ubihydroquinone oxidation, and for the formalism developed here to describe these reactions.
   There is obviously some degree of arbitrariness in the particular choice of values for driving force for the first electron transfer reaction, since the true value for $\Delta G^{overall}$ is not known. Nevertheless, the general pattern shown in Fig. 4 would be expected to apply to all plausible choices, and the explanation of the anomalous behavior in strain Y156W would hold in any case.
3. The curves of Fig. 4 bring up another issue, which relates to the slopes observed. The choice of driving force determines what parameters of the equation are needed to shift the curves till they intercept the experimental values, and hence determines the slope at the intercept. Hong et al. [21] have an exhaustive discussion of this question, and some additional points are covered in Ref. [36]. From the arguments presented there, it seems very likely that the first electron transfer is uphill, but how much so is debatable. In principle, the data from mutant strains provide constraints (dependent on model) on the choice; however, they should perhaps be treated with some caution, since the rate of electron transfer can obviously be changed by more pleiotrophic effects than the direct dependence on driving force. Nevertheless, taken at face value, the data suggest that a classical Marcus treatment gives a better fit than the Moser et al. treatment. If further experiments reinforce this conclusion, the difference might show to what extent the quantum mechanical complexities implied in the Moser et al. treatment [69] are necessary.

The reaction of QH_2 oxidation at the Q_o-site proceeds beyond the first electron step because the overall equilibrium constant for the two electron process is favorable, and because the reduced heme b_L product is rapidly removed by electron transfer to heme b_H and the Q_i-site. Because the overall rate seems to be independent of the driving force for the second electron transfer within the range for which data are available, the rate is clearly not limiting, and likely in practice to be determined by a rate constant much higher than that for the first electron transfer. The kinetic complexity introduced by the bifurcation of electron transfer provides some fascinating physical chemistry, as discussed elsewhere [21,36]. The program used for examination of the parameters for the first electron transfer also generates Marcus curves for the second electron transfer, from SQ to heme b_L, using calculated values for driving force derived from the need for thermodynamic consistency between the partial and overall processes, as described previously [21]. The distance for the second electron transfer is strongly model-dependent. The main kinetic requirement is for a combination of rate constant and occupancy of the SQ intermediate state that gives a rate sufficiently in excess of the limiting rate to explain the lack of effect of driving force for this reaction [21]. The program (in executable and Visual Basic source code forms) is available at URL http://www.life.uiuc.edu/crofts/Marcus_Bronsted/, and will allow readers to explore these parameters themselves.

A plausible reaction energy profile, based on the fit shown by curve C and values for the second electron transfer that satisfy the conditions above, is shown in Fig. 5. This illustrates the main points made above. The binding energies for formation of the ES-complex have been estimated, and are relatively small, thus avoiding a kinetic trap. Transfer of the first electron from QH_2 to ISP_{ox} involves co-transfer of a H^+, and is formally a H-transfer. The activation barrier is high, and partitioned into two steps. The first of these is an unfavorable intermediate step in which the proton transfer through the H-bond sets up a suitable configuration for electron transfer. Electron transfer has to overcome an additional barrier, and this governs the dependence on E_m ISP. The first electron (H) transfer reaction is overall unfavorable, but the step involving electron transfer is nearly isopotential. The slow rate of the first electron transfer is determined by the low occupancy of the intermediate proton configuration, and an electron transfer step that has a high rate constant and low reorganization energy in line with expectations based on the distance involved. The positive overall ΔG for the first electron transfer ensures that the SQ intermediate is maintained at a low concentration, and minimizes the likelihood of by pass reactions, including reaction with O_2 to generate damaging reactive oxygen species. The reaction is pulled

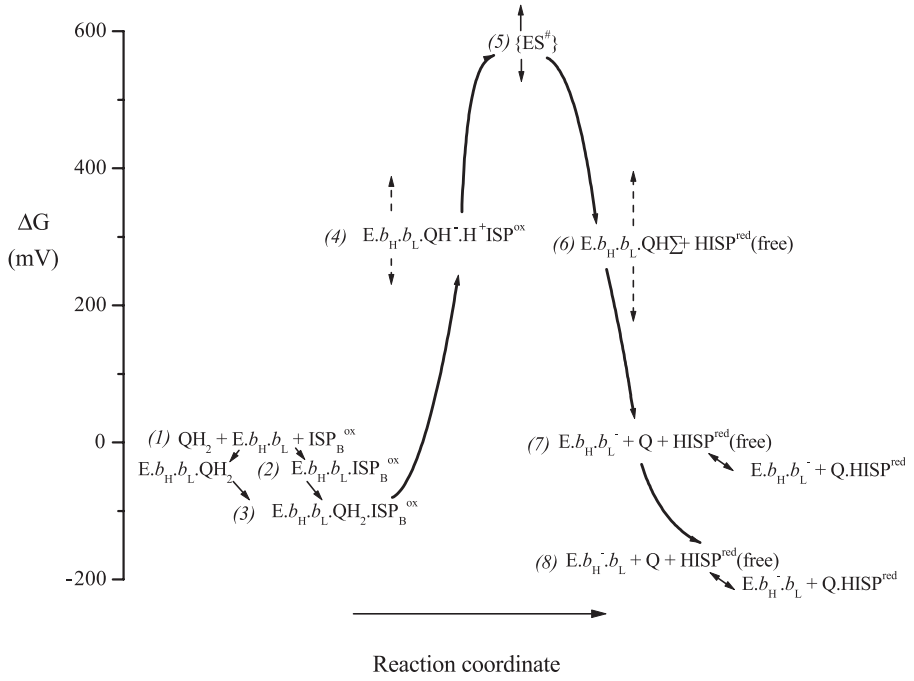

Fig. 5. The energy profile for the oxidation of QH_2 at the Q_o-site, based on the parameters discussed in the text. The states are numbered as follows:

(1) The reactants
(2) alternative intermediate states
(3) the ES-complex (see Scheme 1)
(4) The proton-transfer state needed for electron transfer
(5) The activated state
(6) The intermediate product state after the first electron transfer
(7) The product state after the second electron transfer, shown in equilibrium with the $g_x = 1.80$ complex
(8) The product state after electron transfer to heme b_H (as observed in the presence of antimycin), also shown in equilibrium with the $g_x = 1.80$ complex.

The vertical arrows emphasize the fact that exact values for energy levels of intermediate states are not known.

over by the very rapid transfer of the second electron to heme b_L, and a favorable equilibrium constant arising from the further electron transfer to heme b_H and then to Q or SQ as terminal acceptor at the Q_i-site. A detailed discussion of the second electron transfer reaction is beyond the cope of this paper, but is covered elsewhere [21,36].

Acknowledgements

Although Jerry Babcock did not work on the bc_1 complex system, he was very much a guiding force and mentor in my introduction to proton-coupled electron transfer reactions. He introduced me to the important kinetic implications of the coupling, to the work of his colleague Dan Nocera on the model systems that provided essential insights to the controlling effect of the proton transfer, and to the review article by Cukier and Nocera in which they discussed the application of Marcus theory to proton-coupled electron transfer. In more general terms, for those of us less gifted, Jerry had the happy ability to discuss difficult physicochemical topics and to unmask the underlying simplicities, without making us feel inadequate. We all miss him.

References

[1] Z. Zhang, L.-S. Huang, V.M. Shulmeister, Y.-I. Chi, K.-K. Kim, L.-W. Hung, A.R. Crofts, E.A. Berry, S-H. Kim, Nature (Lond.) 392 (1998) 677–684.
[2] C.-A. Yu, J.-Z. Xia, A.M. Kachurin, L. Yu, D. Xia, H. Kim, J. Deisenhofer, Biochim. Biophys. Acta 1275 (1996) 47–53.
[3] D. Xia, C.-A. Yu, H. Kim, J.-Z. Jia-Zhi Xia, A.M. Kachurin, L. Zhang, L. Yu, J. Deisenhofer, Science 277 (1997) 60–66.
[4] S. Iwata, J.W. Lee, K. Okada, J.K. Lee, M. Iwata, B. Rasmussen, T.A. Link, S. Ramaswamy, B.K. Jap, Science 281 (1998) 64–71.
[5] H. Kim, D. Xia, C.A. Yu, J.Z. Xia, A.M. Kachurin, L. Zhang, L. Yu, J. Deisenhofer, Proc. Natl. Acad. Sci. U. S. A. 95 (1998) 8026–8033.
[6] C.-A. Yu, D. Xia, H. Kim, J. Deisenhofer, L. Zhang, A. Kachurin, L. Yu, Biochim. Biophys. Acta 1365 (1998) 151–158.
[7] C. Hunte, J. Koepke, C. Lange, T. Roßmanith, H. Michel, Structure 8 (2000) 669–684.
[8] A.R. Crofts, C.A. Wraight, The electrochemical domain of photosynthesis, Biochim. Biophys. Acta 726 (1983) 149–186.
[9] A.R. Crofts, S.W. Meinhardt, K.R. Jones, M. Snozzi, Biophys. Acta 723 (1983) 202–218.
[10] S.W. Meinhardt, A.R. Crofts, FEBS Lett. 149 (1982) 223–227.
[11] S.W. Meinhardt, A.R. Crofts, Biochim. Biophys. Acta 723 (1983) 219–230.
[12] E.G. Glaser, A.R. Crofts, Biochim. Biophys. Acta 766 (1984) 322–333.

[13] E.G. Glaser, S.W. Meinhardt, A.R. Crofts, FEBS Lett. 178 (1984) 336–342.
[14] A.R. Crofts, in: A.N. Martonosi (Ed.), The Enzymes of Biological Membranes, vol. 4. Plenum, New York, 1985, pp. 347–382.
[15] A.R. Crofts, in: Govindjee (Ed.), The Q-cycle, -a personal perspective. In: The Millenium Issues on the History of Photosynthesis, Photosynth. Res., 2004, in press.
[16] A.R. Crofts, S.J. Hong, N. Ugulava, B. Barquera, R.B. Gennis, M. Guergova-Kuras, E. Berry, Proc. Natl. Acad. Sci. U. S. A. 96 (1999) 10021–10026.
[17] S. Izrailev, A.R. Crofts, E.A. Berry, K. Schulten, Biophys. J. 77 (1999) 1753–1768.
[18] A.R. Crofts, M. Guergova-Kuras, L.-S. Huang, R. Kuras, Z. Zhang, E.A. Berry, Biochemistry 38 (1999) 15791–15806.
[19] A.R. Crofts, S. Hong, Z. Zhang, E.A. Berry, Biochemistry 38 (1999) 15827–15839.
[20] A.R. Crofts, B. Barquera, R.B. Gennis, R. Kuras, M. Guergova-Kuras, E.A. Berry, Biochemistry 38 (1999) 15807–15826.
[21] S.J. Hong, N. Ugulava, M. Guergova-Kuras, A.R. Crofts, J. Biol. Chem. 274 (1999) 33931–33944.
[22] E. Berry, M. Guergova-Kuras, L.-S. Huang, A.R. Crofts, Ann. Rev. Biochem. 69 (2000) 1007–1077.
[23] A.R. Crofts, E.A. Berry, R. Kuras, M. Guergova-Kuras, S. Hong, N. Ugulava, in: G. Garab (Ed.), Photosynthesis: Mechanisms and Effects, vol. III. Kluwer Academic, Dordrecht, 1998, pp. 1481–1486.
[24] M. Brugna, S. Rodgers, A. Schricker, G. Montoya, M. Kazmeier, W. Nitschke, I. Sinning, Proc. Natl. Acad. Sci. U. S. A. 97 (2000) 2069–2074.
[25] H. Tian, L. Yu, M.W. Mather, C.-A. Yu, J. Biol. Chem. 273 (1998) 27953–27959.
[26] H. Tian, S. White, L. Yu, C.-A. Yu, J. Biol. Chem. 274 (1999) 7146–7152.
[27] K. Xiao, L. Yu, C.A. Yu, J. Biol. Chem. 275 (2000) 38597–38604.
[28] E. Darrouzet, M. Valkova-Valchanova, C.C. Moser, P.L. Dutton, F. Daldal, Proc. Natl. Acad. Sci. U. S. A. 97 (2000) 4567–4572.
[29] J.H. Nett, C. Hunte, B.L. Trumpower, Eur. J. Biochem. 267 (2000) 5777–5782.
[30] V.H. Obungu, Y. Wang, S.M. Amyot, C.B. Gocke, D.S. Beattie, Biochim. Biophys. Acta 1457 (2000) 36–44.
[31] K. Xiao, A. Chandrasekaran, L. Yu, C.A. Yu, J. Biol. Chem. 276 (2001) 46125–46131.
[32] A.R. Crofts, E.A. Berry, Curr. Opin. Struck. Biol. 8 (1998) 501–509.
[33] C. Hunte, FEBS Lett. 504 (2001) 126–132.
[34] E. Darrouzet, C.C. Moser, P.L. Dutton, F. Daldal, TIBS 26 (2001) 445–451.
[35] N.B. Ugulava, A.R. Crofts, FEBS Lett. 440 (1998) 409–413.
[36] A.R. Crofts, The Cytochrome bc_1 Complex Function in the Context of Structure, Annu. Rev. Physiol. (2004) in press.
[37] M. Guergova-Kuras, R. Kuras, N. Ugulava, I. Hadad, A.R. Crofts, Biochemistry 39 (2000) 7436–7444.
[38] A.R. Crofts, M. Guergova-Kuras, R. Kuras, N. Ugulava, J. Li, S. Hong, Biochim. Biophys. Acta 1459 (2000) 456–466.
[39] A. Crofts, M. Guergova-Kuras, N. Ugulava, R. Kuras, S. Hong, Proton processing at the Q_o-site of the bc_1 complex of *Rhodobacter sphaeroides*. Proc. XIIth Congress of Photosynthesis Research, (2002) S12-002, six pages.
[40] C. Snyder, B.L. Trumpower, Biochim. Biophys. Acta 1365 (1998) 125–134.
[41] P.R. Rich, D.S. Bendall, Biochim. Biophys. Acta 5932 (1981) 506–518.
[42] T.A. Link, FEBS Lett. 412 (1997) 257–264.
[43] U. Brandt, FEBS Lett. 387 (1996) 1–6.
[44] U. Brandt, J.G. Okun, Biochemistry 36 (1997) 11234–11240.
[45] T.A. Link, G. von Jagow, J. Biol. Chem. 270 (1995) 25001–25006.
[46] R. Covián, R. Moreno-Sánchez, Eur. J. Biochem. 268 (2001) 5783–5790.
[47] V.P. Shinkarev, D.R.J. Kolling, T.J. Miller, A.R. Crofts, Biochemistry 41 (2002) 14372–14382.
[48] T.A. Link, Adv. Inorg. Chem. 47 (1999) 83–157.
[49] C. Colbert, M.M.-J. Couture, L.D. Eltis, J.T. Bolin, Structure 8 (2000) 1267–1278.
[50] G.M. Ullmann, L. Noodleman, D.A. Case, J. Biol. Inorg. Chem. 7 (2002) 632–639.
[51] S. De Vries, S.P.J. Albracht, F.J. Leeuwerik, Biochim. Biophys. Acta 546 (1979) 316–333.
[52] H. Ding, D.E. Robertson, F. Daldal, P.L. Dutton, Biochemistry 31 (1992) 3144–3158.
[53] H. Ding, C.C. Moser, D.E. Robertson, M.K. Tokito, F. Daldal, P.L. Dutton, Biochemistry 34 (1995) 15979–15996.
[54] R.E. Sharp, A. Palmitessa, B.R. Gibney, J.L. White, C.C. Moser, F. Dutton, P.L. Dutton, Biochemistry 38 (1999) 3440–3446.
[55] S. Iwata, M. Saynovits, T.A. Link, H. Michel, Structure 4 (1996) 567–579.
[56] R.I. Samoilova, D. Kolling, T. Uzawa, T. Iwasaki, A.R. Crofts, S.A. Dikanov, J. Biol. Chem. 277 (2002) 4605–4608.
[57] J.R. Bowyer, P.L. Dutton, R.C. Prince, A.R. Crofts, Biochim. Biophys. Acta 592 (1980) 445–460.
[58] T.A. Link, U. Haase, U. Brandt, G. von Jagow, J. Bioenerg. Biomembranes 25 (1993) 221–232.
[59] A.R. Crofts, V.P. Shinkarev, S.A. Dikanov, R.I. Samoilova, D. Kolling, Biochim. Biophys. Acta 1555 (2002) 48–53.
[60] R.E. Sharp, B.R. Gibney, A. Palmitessa, J. White, J.A. Dixon, C.C. Moser, F. Daldal, P.L. Dutton, Biochemistry 38 (1999) 14973–14980.
[61] E. Darrouzet, M. Valkova-Valchanova, F. Daldal, J. Biol. Chem. 277 (2002) 2464–3470.
[62] C.-A. Yu, X. Wen, K. Xiao, D. Xia, L. Yu, Biochim. Biophys. Acta 1555 (2002) 65–70.
[63] W.M. Clark, Oxidation Reduction Potentials In Biological Systems, Krieger, New York, 1973, p. 584.
[64] A.R. Crofts, Z. Wang, Photosynth. Res. 22 (1989) 69–87.
[65] D.L. Gatti, S.W. Meinhardt, T. Ohnishi, A.J. Tzagoloff, Mol. Biol. 205 (1989) 421–435.
[66] E. Denke, T. Merbitzzahradnik, O.M. Hatzfeld, C.H. Snyder, T.A. Link, B.L. Trumpower, J. Biol. Chem. 273 (1998) 9085–9093.
[67] T. Schröter, O.M. Hatzfeld, S. Gemeinhardt, M. Korn, T. Friedrich, B. Link, T. Link, Eur. J. Biochem. 255 (1998) 100–106.
[68] S.R. Van Doren, R.B. Gennis, B. Barquera, A.R. Crofts, Biochemistry 32 (1993) 8083–8091.
[69] C.C. Moser, C.C. Page, R. Farid, P.L. Dutton, J. Bioenerg. Biomembranes 27 (1995) 263–274.
[70] D. DeVault, Q. Rev. Biophys. 13 (1980) 387–564.
[71] G. Engstrom, K. Xiao, C.-A. Yu, L. Yu, B. Durham, F. Millett, J. Biol. Chem. 277 (2002) 31072–31078.
[72] J.A. Roberts, J.P. Kirby, S.T. Wall, D.G. Nocera, Inorg. Chim. Acta 263 (1997) 395–405.
[73] R.I. Cukier, D.G. Nocera, Annu. Rev. Phys. Chem. 49 (1998) 337–369.
[74] M.S. Graige, M.L. Paddock, G. Feher, M.Y. Okamura, Biochemistry 38 (1999) 11465–11473.
[75] A.J. Kresge, D.N. Silverman, Methods Enzymol. 308 (1999) 276–297.
[76] E. Pines, B.-Z. Magnes, M.J. Lang, G.R. Fleming, Chem. Phys. Lett. 281 (1997) 413–420.
[77] V.L. Davidson, Biochemistry 35 (1996) 14036–14039.
[78] R.A. Marcus, N. Sutin, Biochim. Biophys. Acta 811 (1985) 265–322.
[79] S. Junemann, P. Heathcote, P.R. Rich, J. Biol. Chem. 273 (1998) 21603–21607.
[80] C.C. Moser, J.M. Keske, K. Warncke, R.S. Farid, P.L. Dutton, Nature 355 (1992) 796–802.